Biomaterials 140 (2017) 138–149

Contents lists available at ScienceDirect

Biomaterials

journal homepage: www.elsevier.com/locate/biomaterials

Apatite nanoparticles strongly improve red blood cell cryopreservation by mediating trehalose delivery via enhanced membrane permeation

Martin Stefanic [a, e, **], Kevin Ward [a], Harvey Tawfik [b], Ralf Seemann [b], Vladimir Baulin [c, ***], Yachong Guo [c], Jean-Baptiste Fleury [b, ****], Christophe Drouet [d, *, 1]

[a] Biopharma Technology Limited, Winchester SO23 0LD, United Kingdom
[b] Universitat des Saarlandes, Experimental Physics, 66123 Saarbruecken, Germany
[c] Universitat Rovira i Virgili (URV), Tarragona 43007, Spain
[d] CIRIMAT Institute, Université de Toulouse, CNRS, INPT, UPS, Ensiacet, 4 allée E. Monso, 31030 Toulouse, France
[e] Advanced Materials Department, Jozef Stefan Institute, 1000 Ljubljana, Slovenia

ARTICLE INFO

Article history:
Received 6 May 2017
Received in revised form
14 June 2017
Accepted 15 June 2017
Available online 18 June 2017

Keywords:
Red blood cells
Membrane permeation
Apatite
Nanoparticles
Cryopreservation
Lipid bilayer

ABSTRACT

Cryopreservation of red blood cells (RBC) is an important method for maintaining an inventory of rare RBC units and managing special transfusion circumstances. Currently, in a clinical setting, glycerol is used as cryoprotectant against freezing damage. After thawing and before transfusion, glycerol must however be removed to avoid intravascular hemolysis, via a complex and time-consuming deglycerolization process which requires specialized equipment. Improved cryopreservation methods using non-toxic agents are required to increase biocompatibility and decrease processing time. Biocompatible cryoprotectants (e.g. trehalose) were proposed, but their low permeation through RBC membranes limits their cryoprotection efficacy. Herein, we report for the first time a glycerol-free cryopreservation approach, using colloidal bioinspired apatite nanoparticles (NP) as bioactive promoters of RBC cryopreservation mediated by trehalose. Addition of apatite NP in the medium tremendously increases RBC cryosurvival, up to 91% (42% improvement compared to a control without NP) which is comparable to FDA-approved cryoprotection protocol employing glycerol. NP concentration and incubation conditions strongly modulate the NP bioactivity. Complementary experimental and computational analyses of the interaction between apatite NP and model lipid bilayers revealed complex events occurring at the NP-bilayer interface. Apatite NP do not cross the bilayer but momentarily modulate its physical status. These changes affect the membrane behavior, and promote the permeation of trehalose and a model fluorescent molecule (FITC). This approach is a new alternative to using toxic glycerol for cells cryopreservation, and the identification of this enhancing no-pore permeation mechanism of apatite NP appears as an original delivery pathway for cryoprotectant agents and beyond.

1. Introduction

Transfusion of red blood cells (RBC) is essential for patients necessitating blood supplies [1], in particular after traumas or surgical procedures, but also in cases of blood-related pathologies such as anemia or leukemia [2]. Viable RBC supplies must be ensured by blood banks, requiring the setup of cell preservation methodologies [3,4]. Low-temperature approaches allow reaching high rates of cell preservation [5,6], up to 85–90%; however, current approved RBC cryopreservation methods require high concentrations of glycerol as cryoprotective agent (e.g. 40% w/v in

* Corresponding author.
** Corresponding author. Present address: Advanced Materials Department, Jozef Stefan Institute, 1000 Ljubljana, Slovenia.
*** Corresponding author.
**** Corresponding author.
E-mail addresses: martin.stefanic@gmail.com (M. Stefanic), va.baulin@gmail.com (V. Baulin), jean-baptiste.fleury@physik.uni-saarland.de (J.-B. Fleury), christophe.drouet@cirimat.fr (C. Drouet).
[1] ResearcherID: A-8023-2008.

http://dx.doi.org/10.1016/j.biomaterials.2017.06.018
0142-9612/

North America) [2]. Glycerol has been studied as cryoprotectant for RBC cryopreservation for decades and its efficacy as cryoprotectant, the mechanism of its protecting ability, as well as its effects on cells, tissues and patients as a whole have been well documented [6–8]. However, because of the toxicity of glycerol, which can generate side effects such as hemolysis or RBC shape alterations [9], the use of cryopreserved RBC for transfusion necessitates a complex and lengthy procedure of deglycerolization prior to the use in patients [10]. This deglycerolization process requires multiple washing steps where about 15% cells are hemolyzed [6]. Also, published studies pointed out the adverse changes in RBC morphology after cryopreservation and deglycerolization [10,11]. Moreover, glycerol residues remain inside the cells despite this post-treatment (<1% for North America and <0.8% for Europe) [6], which can provoke complications in some patients. These considerations prevent the widespread development of cryoprotective approaches for providing large quantities of RBC to hospital units in minimal timescales [4]. Nowadays such approaches are limited to rare blood types.

Thus, improved cryopreservation methods based on non-toxic cryoprotective additives which would not require long post-processing are needed to optimize RBC preservation and allow better availability of blood to patients.

Alternative biocompatible cryoprotectants including biopolymers such as polyvinylalcohol (PVA) [12] or sugars [13–15] like trehalose have been proposed, but their cryoprotective abilities remain limited [12] for practical relevance and approval from regulatory commissions (expected survival typically > 80%) [2]. Trehalose is a particularly appealing bio-inspired cryoprotectant as it is well known for its role in protecting cells and organisms against a variety of stresses, including freezing, desiccation, heat shock, oxidative and osmotic stresses [16,17]. However, in order to provide maximum protection, trehalose must be present on both sides of the cell membrane; yet it has very low permeability to RBC membrane under normal conditions [16]. Therefore, research has focused on methods for delivering trehalose into cells, i.e. via the use of trehalose-loaded liposomes [15], membrane-permeable biopolymers [13], electro-permeabilization [18], and chemical methods [16], but research is still in progress for attaining high cell recovery after freeze-thawing.

So far, there have been no reports on the use of inorganic-based compounds for the delivery of trehalose into cells. Yet, bioactive and biocompatible inorganics have already been found particularly useful in various biomedical domains (e.g. nanomedicine, medical imaging/theranostic, regenerative medicine, etc.) [19,20]. Possible inorganic compounds for delivery of trehalose to RBC could be calcium phosphates (CaP), which are known for their excellent biocompatibility, biodegradability and bioactivity [21–24]. Moreover, it was demonstrated that biomimetic (bone-like) apatite nanoparticles (NP), which possess structural and chemical similarity with the mineral component of bones and dentin [25], are particularly efficient carriers of drugs and nucleic acids into various types of cells, making them a promising candidate for further investigations as nanocarriers of payloads in cells [22,26–29]. The proposed mechanism of apatite NP assisted delivery of bioactive molecules in cells is generally based on endocytosis-mediated transport. However, endocytosis does not exist in mature mammal RBC [30], meaning that delivery of trehalose into RBC assisted by apatite nanoparticles should occur via a different mechanism, for example via a local modification of RBC membrane physical properties. The nano-size and charge distribution of apatite particles may modulate their interaction with RBC cells [31], although this was reported so far only for the specific case of heparin-coated hydroxyapatite, in another scientific context, and in the absence of cryoprotectants. To-date the possibility to use apatite NP for enhancing RBC survival has not been investigated.

Previous work has shown that apatite nanoparticles could be formulated as colloidal suspensions via the formation of an external organic corona surrounding the particles. 2-aminoethylphosphate (AEP) as well as phosphonated polyethyleneglycol have been shown to be efficient stabilizing agents to form individualized colloidal apatite NP [23,28]. In the case of AEP-stabilized apatite NP, positively-charged particles are obtained due to the presence of an amino group on the AEP molecule; however the addition of hexametaphosphate (HMP) anions was found to improve significantly the dispersibility of the particles, facilitate their purification (e.g. via dialysis process) and favor colloidal stability [22,32]. This effect can be explained by the organization of HMP anions around the AEP-stabilized particles, thus leading to the formation of a double-layer (positive/negative) organic corona on the surface of apatite NP as illustrated in Fig. 1a.

Because of this peculiar distribution of positive and negative charges around the particles, AEP/HMP-stabilized apatite NP might lead to specific interactions with cell membranes, possibly modulating momentarily the properties of the membrane, which could in turn promote the permeation of trehalose (see general concept on Fig. 1b). Based on this hypothesis, and taking into account good hemocompatibility of colloidal apatite NP [33], the aim of the present work was to investigate, for the first time, the possibility of using AEP/HMP-stabilized colloidal apatite nanoparticles for facilitating the delivery of trehalose into RBC, in view of promoting their cryopreservation without the use of glycerol. This paper reports experimental data on the role of colloidal apatite NP on RBC viability after freeze-thawing cycle and explores, at the molecular scale and by using synthetic lipid bilayers, the mechanism of interactions between RBC and apatite NP. These experiments were completed by the use of computational methods, with the aim to explain our experimental observations. The set of complementary data is presented and discussed, to demonstrate the active role of colloidal apatite NP for RBC cryopreservation.

2. Results

2.1. Characterization of the colloidal apatite nanoparticles used in this work

After preparation, the AEP/HMP-stabilized colloidal nanoparticles (NP) prepared (see Materials and Methods section) were characterized from a physico-chemical viewpoint using complementary techniques. DLS measurements indicated that the mean NP size followed a monomodal distribution centered on d_{50} ~ 40 nm (Fig. 2a), with d_{10} ~ 22 nm and d_{90} ~ 80 nm.

Zeta potential measurements systematically showed an overall negative surface potential of the order of −50 to −55 mV. This can be explained by the exposure of HMP anions organized on the organic corona at the periphery of the particles, and covering the positively charged AEP adsorbed molecules (Fig. 1a) [22]. XRD analyses pointed out the apatitic nature of the particles by comparison to reference data [25,34], and no additional crystalline compound was detected indicating that the samples are single-phased (Fig. 3a). FTIR results corroborated XRD conclusions by the presence of characteristic phosphate vibration modes related to calcium phosphate apatite (Fig. 3b) [35]. The clear detection (Fig. 3c) of HPO_4^{2-} vibrational contributions in the region 530-550 cm^{-1} (as well as at ~ 875 cm^{-1}), as in bone mineral [25], along with the limited contribution of OH^- ions at 632 cm^{-1} are indicative of the nonstoichiometric character of the apatite phase [25], pointing to the bio-inspired nature of these particles. A low degree of carbonation (arising from atmospheric CO_2) may also be detected in the region 1400-1600 cm^{-1}, corresponding to ~ 1 wt. % carbonate

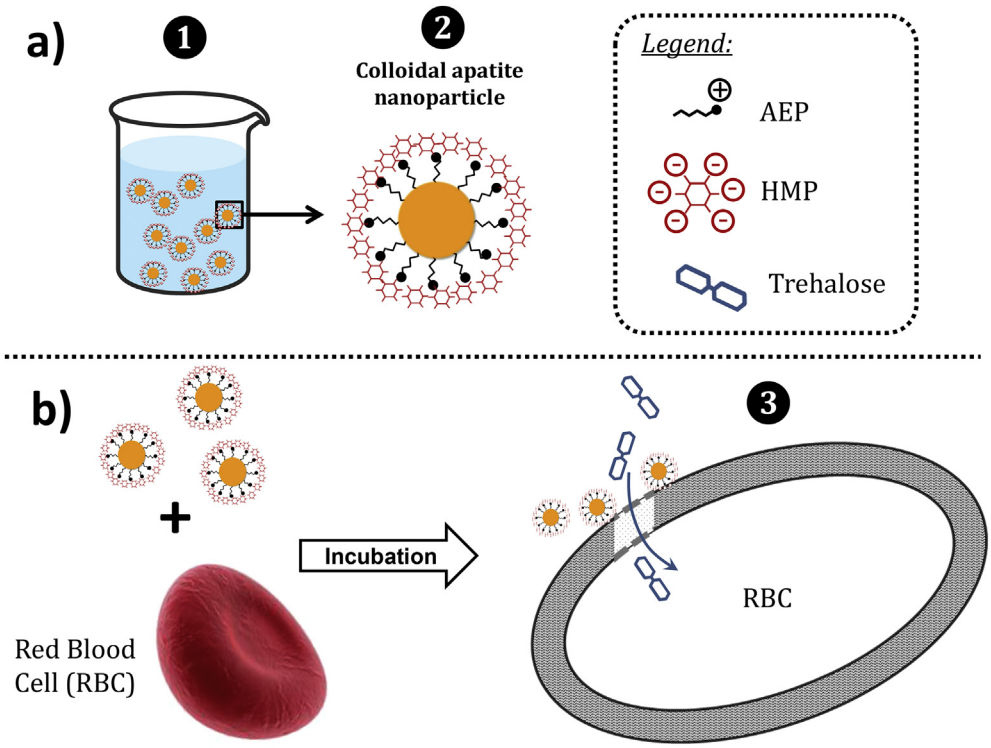

Fig. 1. Schematic description of a) aqueous colloidal suspension ❶ and colloidal AEP/HMP-stabilized apatite nanoparticle ❷, and b) of general concept of enhanced trehalose permeation into red blood cells (RBC) assisted by colloidal apatite nanoparticles.

content (a larger degree of carbonation as in mature bone was not selected here for not complexifying the system). The presence of organic groups arising from the presence of adsorbed AEP was evidenced on FTIR spectra, especially with a band at 754 cm^{-1} characteristic of the $Ca^{2+}_{(surface)}$/AEP interaction (Fig. 3b) [28]. The amount of AEP adsorbed on the NP was measured and corresponded to an AEP/apatite molar ratio of ~0.8%. The HMP added to the colloid represented, on the other hand, an HMP/apatite molar ratio of ~1.4%. The chemical composition of the (nonstoichiometric) apatite phase in the NP was found, from calcium and phosphate titrations and carbonation evaluation, to approach the overall formula $Ca_{8.5}(PO_4)_{4.5}(HPO_4)_{1.4}(CO_3)_{0.1}(OH)_{0.5}$, which as expected departs from the composition of stoichiometric hydroxyapatite and is in contrast close to that of bone mineral [36], thus stressing again the bio-inspired character of this phase. TEM observations of the colloidal NP were in good accordance with DLS data, showing ellipsoidal-like nanoparticles with a length typically around 40 nm and a width of about 10 nm (Fig. 2b).

It may be noted that similar results were found for Eu-free and for Eu-doped apatite samples (where the experimental Eu/(Ca + Eu) molar ratio reached 2.0%).

2.2. Hemolysis of RBC in different incubation media

Incubation of RBC in different incubation media (compositions reported in Table 1) resulted in rather similar levels of hemolysis, in all cases lower than 8% (Table 2). Incubation with apatite NP at pH 6.5 and 7.4 for 7 h resulted in the hemolysis of 7.8 ± 1.2% and 6.1 ± 1.4%, respectively. Although these values are slightly higher compared to RBC in trehalose alone (without NP, 5.6 ± 1.9%) or in

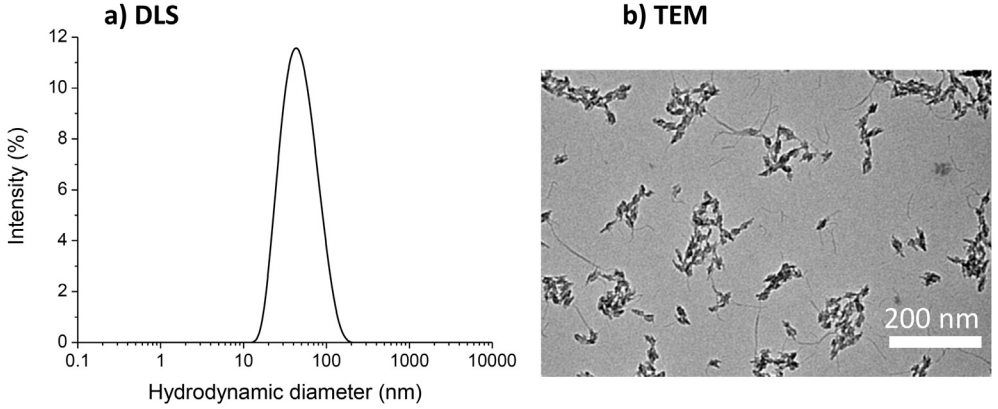

Fig. 2. AEP/HMP-stabilized apatite colloidal NP: a) particle size distribution (hydrodynamic diameters from DLS data) and b) TEM micrograph.

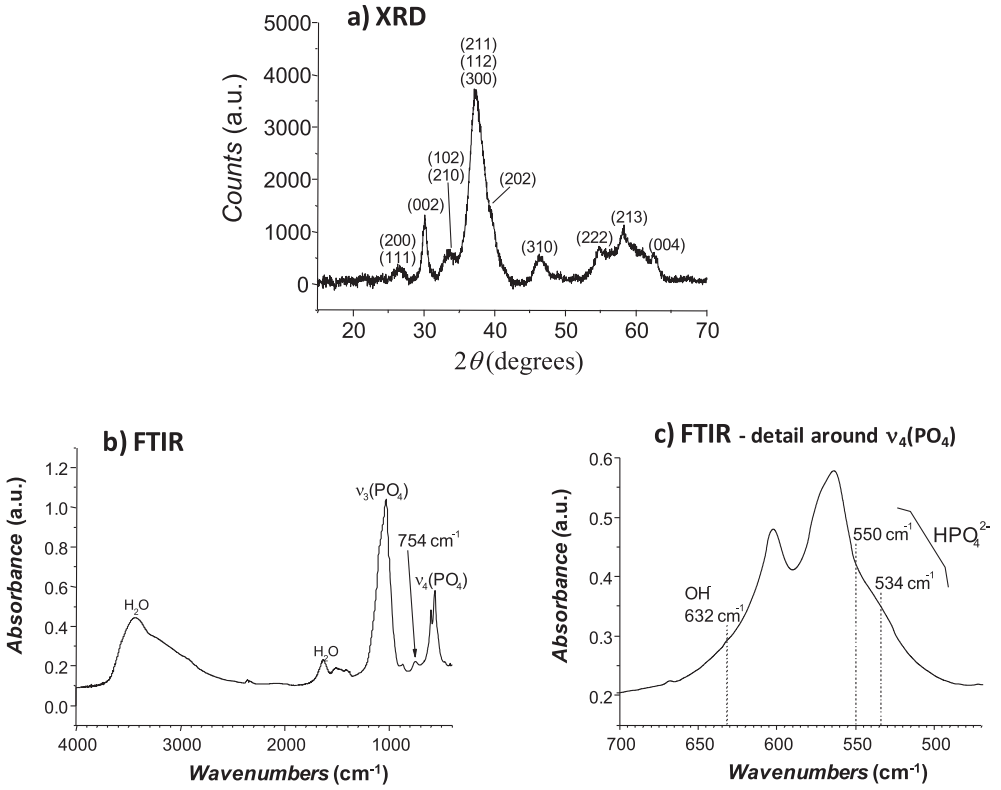

Fig. 3. Complementary analyses of apatite NP used in this work a) XRD pattern, b) FTIR spectrum and c) zoom in the $\nu_4(PO_4)$ domain.

Table 1
Composition of the different incubation media used in this work.

Incubation media	NaCl	Trehalose	"Apa6.5" Apatite NP pH6.5	"Apa7.4" Apatite NP pH7.4
	c (NaCl) = 0.9 wt.% *c* (Hepes) = 20 mM	*c* (NaCl) = 0.5 wt.% *c* (Hepes) = 20 mM *c* (trehalose) = 0.35 M	*c* (NaCl) = 0.5 wt.% *c* (Hepes) = 20 mM *c* (trehalose) = 0.35 M *c* (Apatite) = 2.25 mg/mL	*c* (NaCl) = 0.5 wt.% *c* (Hepes) = 20 mM *c* (trehalose) = 0.35 M *c* (Apatite) = 2.25 mg/mL
pH	7.4	7.4 (or 6.5 when mentioned)	6.5	7.4
Osmolarity (mOsm/L)	320	600	600	600

physiological 0.9% NaCl (4.4 ± 1.1%), the limited degree of hemolysis observed in all cases indicates a good biocompatibility relatively to BRC, which is in agreement with previous data on hemocompatibility of such apatite particles [33].

2.3. Quantification of intracellular trehalose and cryosurvival of RBC after freeze-thawing cycle

The ability for the apatite NP to favor trehalose permeation into live RBC was investigated using a trehalose quantification kit. The results obtained (Fig. 4) clearly point out the increase of intracellular trehalose when apatite NP are present in the incubation

Table 2
Hemolysis of RBC during incubation in different incubation media (see composition in Table 1) for 7 h.

Incubation media	Hemolysis (%)	SD (%)
Apa6.5	7.8	1.2
Apa7.4	6.1	1.4
Trehalose (pH 7.4)	5.6	1.9
NaCl 0.9%	4.4	1.1

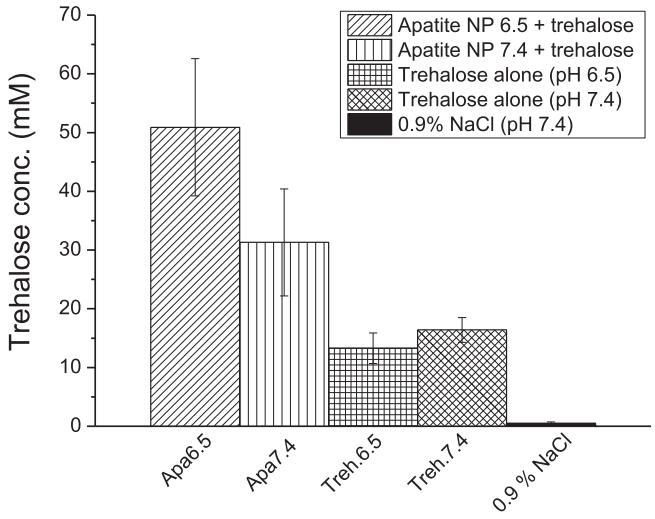

Fig. 4. Intracellular trehalose concentration for RBC incubated in different incubation media. Data were derived from three replicates and error bars represent standard deviations.

medium. In contrast, significantly lower amounts are measured for media containing only trehalose or only NaCl. Noteworthy, a decrease of the incubation pH from 7.4 to 6.5 appears to have a clear enhancing effect on trehalose permeation when apatite NP are present (from 31.3 ± 9.1 up to 50.9 ± 11.7 mM trehalose, respectively). In contrast, no enhancement is observed for trehalose only (about 15 mM trehalose), therefore further experiments run in trehalose-only medium were conducted, for simplification, at physiological pH.

To investigate the direct impact of apatite NP on RBC cryoprotection efficacy, the post freeze-thaw survival of cells incubated in trehalose alone was then compared to the survival of cells incubated in both trehalose and apatite NP (media Apa6.5 and Apa7.4, see compositions on Table 1). In particular, survival of RBC suspended in Apa6.5 was shown to be dramatically improved compared to other incubation media tested (Fig. 5). Incubation in Apa6.5 indeed resulted in survival of 90.7 ± 9.8% while survival of 51.8 ± 6.7% was achieved when RBC were incubated in trehalose alone (Fig. 5). This represents an increase in post-thaw viability of about 42%. In contrast, cryosurvival of RBC suspended in Apa7.4 (58.2 ± 10.1%) was only slightly larger than that of trehalose alone, suggesting that medium pH plays a crucial role in tailoring the bioactivity of apatite NP in terms of RBC cryopreservation. Survival of RBC suspended in NaCl 0.9% alone only reached 3.3 ± 1.7% (Fig. 5).

2.4. Formation of a free-standing lipid bilayer in the presence of apatite NP

Within a microfluidic device and using a variant of the Droplet Bilayer Technique (see experimental section) [37,38], the formation of a free-standing lipid bilayer of monoolein or DOPC via a zipping process was investigated in the presence of increasing concentrations of NP (at pH 6.5 or 7.4). To this aim, the NP were dispersed in two fingers separated by the continuous oily phase (Fig. 6a).

Supplementary data related to this article can be found online at http://dx.doi.org/10.1016/j.biomaterials.2017.06.018.

Combining simultaneous optical microscopy and electrophysiological measurements (using a patch-clamp amplifier), our observations indicated that when the concentration of nanoparticles was greater than $c \sim 4–5$ mg/mL (for both pH values), no bilayer could be produced (as evidenced from optical and electrophysiological measurements). In contrast, for lower NP concentrations in the range of 3 to 0.1 mg/mL, a stable lipid bilayer was obtained, as indicated by measure of the bilayer specific electrical capacitance C_S (see Supporting Information, Fig. S1). The capacitance signal however revealed the presence of strong fluctuations just before achieving the bilayer formation: these fluctuations likely resulted from perturbations due to the adhesive interaction between the NP and lipid molecules. These findings already point out the existence of a non-negligible interaction between the hydrophilic apatite NP and the lipid membrane.

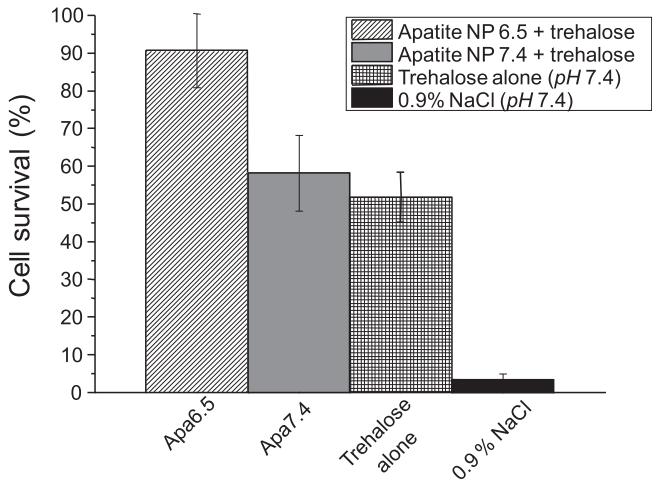

Fig. 5. RBC survival after freeze-thawing in different media (RBC were incubated in media for 7 h at 37 °C prior to freezing).

2.5. Interaction energy between apatite NP and synthetic lipid bilayers

A recently developed method enables extraction of the average free energy of adsorption [39], by using electrophysiological measurements. The method estimates the surface coverage with NP from the change in the magnitude of the electrical capacitance (C_S) plateau as a function of the NP concentration [37]. The lipid bilayer surface coverage can then be plotted as a function of the NP concentration (Fig. 6c): the plots present the shape of a Langmuir isotherm adsorption, assuming a dynamic equilibrium between the free NP in solution and the NP adsorbed to the model membrane. In this model, the surface is considered to have a specific number of sites where the NP can adsorb, and these sites are all equally active, giving rise to a single average value of equilibrium constant K_L. The Langmuir equation gives the relationship between the surface coverage θ and NP concentration c:

$$\theta = \frac{K_L \cdot c}{1 + K_L \cdot c} \quad (1)$$

After obtaining K_L, it becomes possible to estimate the corresponding standard free energy for the adsorption of apatite NP to the surface of the lipid bilayer by the following equation:

$$\Delta G^{\circ} = -RT \ln(K_L) \quad (2)$$

where R is the gas constant (8.314 J K^{-1} mol^{-1}) and T the absolute temperature (in Kelvin).

Following this procedure for the two different media Apa6.5 and Apa7.4, we measured different NP adsorption behaviors depending on the pH value (Table 3).

Results pointed out a larger adsorptive interaction at pH 6.5 compared to pH 7.4, as can be seen on Fig. 5c and from the ΔG° values estimated in Table 3. It may be noted that experiments run with Eu-doped apatite NP led to very similar results, within 5% of variation. These results suggest a greater degree of interaction between the NP (whether doped or not with europium) and the lipid bilayer at slightly acidic pH rather than at physiological value. The order of magnitude of ΔG°, close to −30 kJ mol^{-1}, points to a situation intermediate between physisorption and chemisorption [40,41], indicating a non-negligible degree of interaction.

2.6. Translocation of Eu-doped apatite NP through the lipid bilayer

Translocation of fluorescent Eu-doped apatite NP through the lipid bilayer was followed using a two-droplets system (see details in experimental section). One droplet (left on Fig. 6b) was composed of a medium containing Eu-doped apatite NP (e.g. 0.1 ng/mL), while the second droplet (right on Fig. 6b) was composed of the same medium but without NP. Observation via fluorescence microscopy indicated that the NP, animated by Brownian motion and sometimes interacting with the membrane, systematically remained on the initial compartment (independently of the NP concentration tested) and were not able to passively cross the

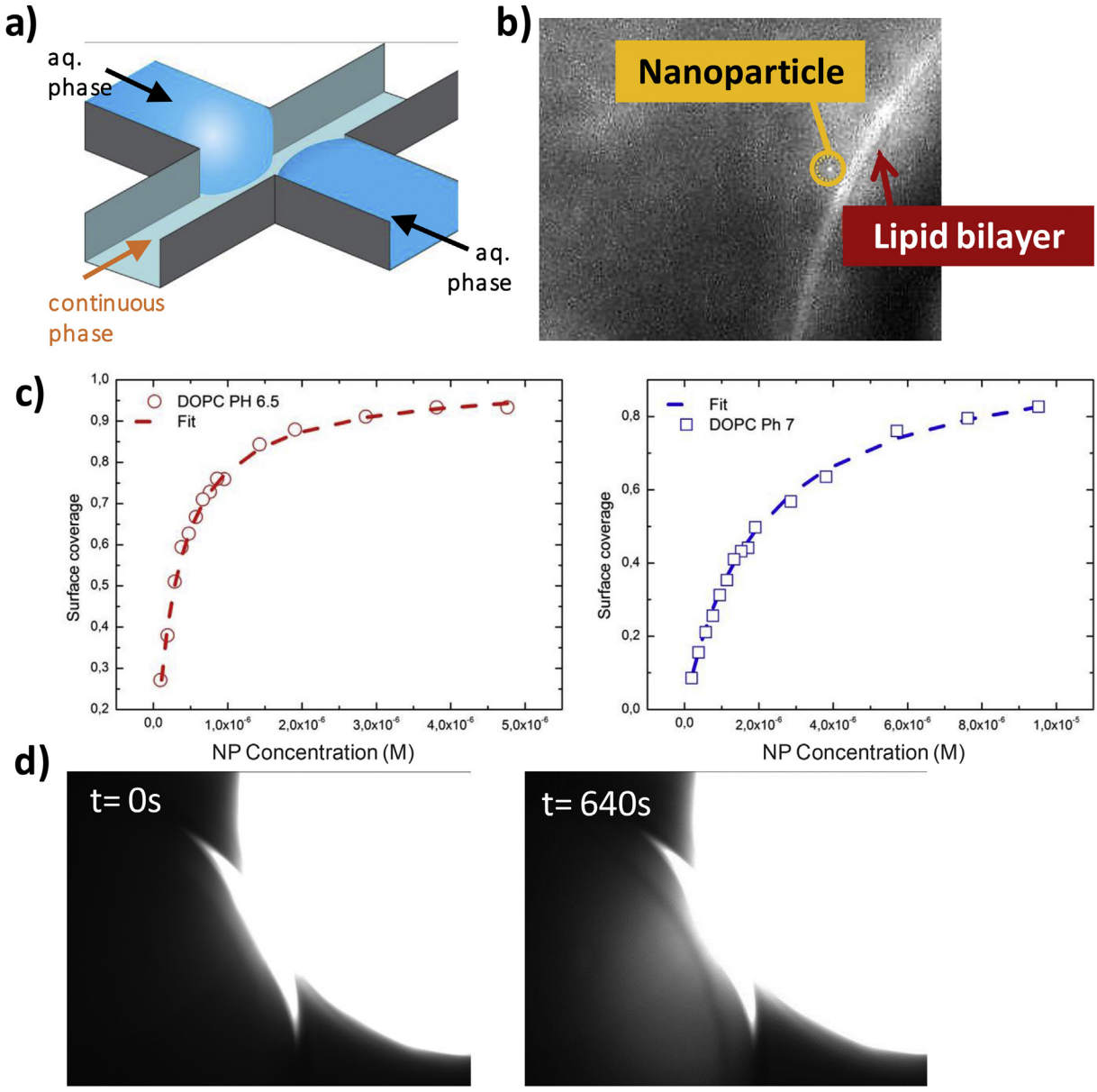

Fig. 6. a) Sketch of the microfluidic cross-channel geometry, displaying two flui rs (aqueous phase in blue) and the oily continuous phase (orange arrow, fluid not shown).b) Epifluorescence micrograph of fluorescing Eu-doped apatite NP next to lipid bilayer (see Video 1 in Supporting Information).c)Langmuir isotherms describing the bilayer coverage as function the NP concentration (for two different pH values of the buffer) determined from bilayer capacitance measurements.d) Micrographs of two water droplets with their interfaces separated by a DOPC lipid bilayer (also see Video 2 in Supporting Information). At the start of the experiment (time = 0 s) the right droplet is full of fluorescent FITC and apatite NP, while the left droplet is just filled with buffer. This image taken at 640 s shows a transfer of FITC from the right droplet to the left droplet in the presence of apatite NP. In the absence of apatite NP, FITC does not diffuse to the left droplet (see Video 3 in Supporting Information). (For interpretation of the references to colour in this figure legend, the reader is referred to the web version of this article.)

Table 3
Calculated values of equilibrium constant (Langmuir) K_L for the system NP/bilayer and related values of the standard free energy of interaction ΔG°.

	pH	K_L (L mol^{-1})	ΔG° (kJ mol^{-1})
DOPC (medium Apa6.5)	6.5	$4 \cdot 10^5$	−32.0
DOPC (medium Apa7.4)	7.4	$1.5 \cdot 10^5$	−29.5

bilayer (see also Video 1 in Supporting Information). Even for experiments performed at high NP concentrations ($c \sim 1$ mg/mL), no particle translocation event was observed even after 8 h of optical observation; and this result was obtained for the 3 pure lipid bilayer compositions monoolein, DOPC and DPHPC.

2.7. Translocation of FITC through the lipid bilayer

Translocation of fluorescent FITC, used as trehalose substitute, through lipid membranes was followed using the two-droplet system (Fig. 6d). One droplet (right on Fig. 5d) contained the medium (either Apa6.5 or Apa7.4) with NP (e.g. 1 mg/mL) and dissolved FITC (2 mM), while the second droplet (left on Fig. 6d) contained the same medium but without NP and FITC. By observing both droplets via fluorescence microscopy, we could follow the FITC transfer across the lipid bilayer over time when apatite NP were present in the medium (see Video 2 in Supporting Information). In addition, the FITC diffusion rate was found to increase with the NP concentration (Fig. S2 in Supporting Information). As can be

observed on Fig. 6d, at the start of the experiment the droplet containing FITC was bright (due to FITC fluorescence) while the droplet without FITC remained dark. After few seconds of incubation, a fluorescent front started to propagate into the dark droplet, and the characteristic shape of a diffusive front emerged in the dark droplet and propagated over time, indicating the translocation of FITC over the lipid membrane (Fig. 6d). It is important to note that FITC translocation was observed only in the presence of apatite NP (with or without Eu doping) and in both media Apa6.5 and Apa7.4; in contrast no diffusion, during the first 15 min, was noticed without apatite particles in the medium (Video 3 in Supporting Information).

Normalizing the brightness in Fig. 6d to the fluorescence signal of the initial FITC concentration in one of the droplets (i.e. 2 mM), we could estimate the translocation rate of FITC molecules across a bilayer to ~0.2 μmol L^{-1} s^{-1} for a monoolein bilayer and to ~0.07 μmol L^{-1} s^{-1} for a DOPC bilayer. The experiments were also repeated for more complex bilayer composition, leading to translocation rates of ~0.05 μmol L^{-1} s^{-1} for an asymmetric DOPC/DPHPC bilayer and of ~0.03 μmol L^{-1} s^{-1} for a "Red Blood Cell-like" composition (see experimental section).

2.8. Computational modeling of the NP/bilayer interaction

The lipid bilayer/apatite nanoparticle interaction was also studied here from a simulation viewpoint, based on the Single Chain Mean Field (SCMF) theory [42,43]. The method has indeed been shown previously to describe adequately the mechanical properties of lipid bilayers [42]. Using a 3-beads model (one head bead H and two tail beads T) to describe lipid bilayer with previously reported parameters [42], the bilayer is represented by the fields of lipid tails (T) and heads (H), which are allowed to rearrange due to local environment and interactions with external objects. Here, the apatite nanoparticle was considered spherical and was modeled as adsorbing to lipid heads (H) through the negative interaction parameter ε_H. This parameter denotes the attraction of lipid heads H to the surface of the NP. Due to the curvature of the NP, a strong attraction of lipid heads toward the surface of NP is generated, leading to the lifting of lipids out of the bilayer plane, as illustrated in Fig. 7.

These calculations thus suggest that the lipid bilayer is not broken down but that the NP/lipid interaction however partly disrupts the upper leaflet of the bilayer at the position of contact between the NP and lipid bilayer. The destabilized bilayer could then lead to enhanced permeability of low-molecular mass components. This mechanism suggests also that the disruption of the bilayer is reversible.

3. Discussion

Incubation of RBC with apatite NP both at pH 6.5 and 7.4 (Table 2) resulted in low levels of hemolysis (<8%). Although slightly larger than for incubation in physiological NaCl solution, these results indicate that the apatite NP studied here are biocompatible with regard to RBC and suitable for applications in blood transfusion. These findings agree well with recent studies where the good hemocompatibility of apatite NP was reported, especially concerning direct contact with RBC [31,33].

The present work was aimed at exploring the possible enhancing role of AEP/HMP-stabilized apatite NP on the cryosurvival of RBC, especially in link with their peculiar surface charge distribution. The goal in the present study was to use colloidal apatite NP since this colloidal state, provided by the stabilizing organic corona, ensures the stability of the suspensions and avoids unwanted post-agglomeration. In this study, we employed

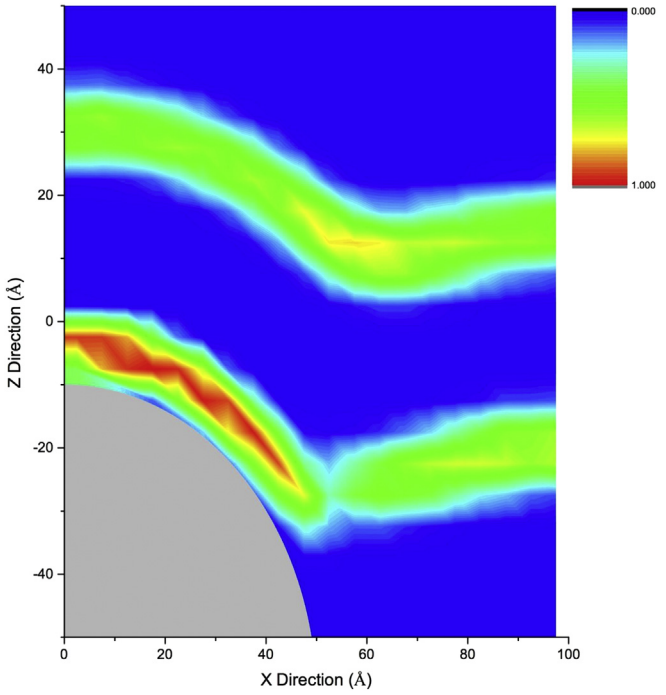

Fig. 7. Single Chain Mean Field Theory calculation of interaction between an apatite NP (hydrophilic) and the lipid bilayer. NP attracts the heads of lipids (density of heads is shown in color: red – high volume fraction, blue – low volume fraction) and destabilizes the lipid bilayer making it more permeable. The diameter of the tip of NP is 10 nm, the attraction parameter is $\varepsilon_H = -7\ K_T$. (For interpretation of the references to colour in this figure legend, the reader is referred to the web version of this article.)

relatively-rapid freezing and thawing in the cryopreservation protocol; indeed previous works have shown that rapid freezing and thawing of RBC resulted in significantly higher survival rates compared to slower protocols [13,14,44]. Our results reveal that the presence of such tailored apatite NP with specific properties (size, surface charge) in the incubation medium increased massively the degree of cryosurvival of RBC in the co-presence of trehalose (Fig. 5). The selection of incubation conditions (pH, ionic strength, NP concentration) was found to be essential for optimizing the bioactivity of apatite NP toward RBC cryosurvival. When RBC were incubated in trehalose-apatite medium at pH 6.5 (medium "Apa6.5"), a survival rate of 91% was reached, which is comparable to the FDA-approved cryopreservation protocol employing glycerol as a cryoprotectant (survival rate 85–90%) [5].

The role of the medium pH was especially found to be significant, as incubation at physiological pH (7.4) decreased the cryosurvival rate from 91 down to about 60%. This pH effect might be related to a modulation of the affinity of molecular species (here lipid moieties) for the surface of apatite. An acidification from 7.4 to 6.5 was previously reported to lead, in the case of DNA adsorption on (non-colloidal) biomimetic apatite [45], to an increased adsorption amount, which was tentatively explained by the release of some HPO_4^{2-} ions from the apatite surface in acidic conditions, in turn favoring the adsorption of the ionic backbone of DNA by providing anchoring surface sites. In the present case, a similar scenario could come into play as well, between lipid heads and apatite particles. Hence, this appears to be validated by our experimental data (Fig. 6c and Table 3), where an increased interaction was detected between the lipid bilayer and apatite nanoparticles at pH 6.5 as compared to pH 7.4, as shown by the differences in membrane capacitance. This effect of pH does not seem to be solely linkable to a change in the organic corona as the

observations reported previously on nucleotide or DNA adsorption enhanced at slightly acidic pH [45] were made on non-colloidal, purely apatitic systems.

Additional evidence of the existence of a strong interaction between apatite NP and the bilayer was shown by investigating the possibility to form free-standing bilayers in the presence of increasing concentrations of NP. Indeed, although the zipping process of the bilayer remained possible for NP concentrations lower than 3 mg/mL, this process became hindered at high NP concentrations. This illustrates an interfering effect of the hydrophilic apatite particles on lipid organization, especially detectable at high NP concentration. An analysis of the capacitance signal during the bilayer zipping process was also carried out, and confirmed the formation of stable bilayers below 3 mg/mL of NP (see Figure S1 in Supporting Information). The presence of fluctuations before bilayer stabilization illustrates perturbations linked to the adhesive interaction between the NP and the lipid molecules. After bilayer formation and reaching a stable capacitance value, the corresponding specific capacitance C_S can be measured so as to follow the effect of the NP. Interestingly, C_S increases with the concentration of apatite NP (Fig. 6c). Theoretically, this increase could indicate a reduction of the corresponding bilayer thickness as $C_S = \frac{\varepsilon_0 \varepsilon_L}{d}$ (e.g. from 2.7 nm for a monoolein bilayer without NP to 2.3 nm with a NP concentration of 1 mg/mL), where ε_L is the dielectric constant of the lipid membrane in the oily phase (squalene), $\varepsilon_L \sim 2.2$ F m^{-1}, and ε_0 is the vacuum permittivity $\varepsilon_0 \sim 8.85.10^{-12}$ F m^{-1} respectively. Although a bilayer thickness reduction does not appear as a probable conclusion in the present case, this capacitance reduction is nonetheless a clear consequence of membrane modification, via the adsorption or insertion of charged nanoparticles into the bilayer. However, these conductivity measurements do not allow directly distinguishing between NP adsorption on the bilayer or partial/complete insertion of NP within the bilayer. In order to examine this point, we performed additional experiments by repeating capacitance measurements when NP were dispersed only on one side of the lipid bilayer (with a concentration ~ 1 mg/mL). During the experiments, a change in the bilayer capacitance was again observed, but decreased by a factor 1.6 compared to the situation where NP were dispersed on both sides of the membrane. These observations indicate that apatite NP do not passively cross the lipid bilayer but rather adsorb on it without being inserted into the bilayer core.

To further confirm that these NP are not able to translocate passively through the bilayer, we set up a novel two-droplet methodology where fluorescent europium-doped apatite NP were dispersed on one side of the bilayer while the other side was composed of the buffer alone. Epifluorescence microscopy analyses then demonstrated (Fig. 6b) that the NP remained on their initial compartment even after several hours of incubation (see also Video 1 in Supporting Information), again validating that such NP cannot passively cross the lipid bilayer.

Our cryosurvival data pointed out however that the presence of apatite NP beside trehalose allowed a significant increase in the RBC cryosurvival as compared to trehalose alone, thus suggesting that more trehalose was able to cross the lipid bilayer in the presence of apatite. Nevertheless, the above results show that apatite NP themselves are not able to translocate through the membrane, despite evident local modifications of the physical/electrical properties of the bilayer. A hypothesis can then be formulated concerning the mechanism of action of the NP, along which these charged NP could facilitate trehalose permeation by altering locally, reversibly and momentarily the membrane properties, providing transient diffusion pathways for trehalose (see schematic view of the concept on Fig. 1b).

In order to validate this hypothesis, we investigated the possible permeation of FITC (a small fluorescent molecule mimicking trehalose) through a DOPC lipid bilayer, in the presence or absence of apatite NP. This set of experiments again used the two-droplet methodology, placing FITC on one side and checking its potential diffusion over time into the other compartment. Fluorescence microscopy clearly indicated the enhanced diffusion of FITC through the lipid bilayer in the presence of apatite NP (Fig. 6d and Video 2 in Supporting Information), and the diffusion rate was found to be function of the NP concentration (Figure S2 in Supporting Information). On the contrary, no FITC detection was recorded in the absence of NP (see Video 3 in Supporting Information). One criticism of this experimental investigation could be that FITC molecules are, in some cases, able to cross some DOPC bilayers [46]; however this process would be slower than the one reported here where a clear activation by apatite NP is detected. Nevertheless, to rebut this point, we also repeated this experiment with membrane compositions that are known to be impermeable to FITC, which is the case for membranes with asymmetric composition like DOPC/DPHPC. Even in this case, we measured again a clear activated transfer of FITC as a function of the NP concentration (Figure S2 in Supporting Information) and attainment of a plateau. These findings offer a strong experimental demonstration of the enhanced permeation of FTIC (mimicking trehalose) when incubation is carried out in the co-presence of our apatite NP.

The increased permeation of FITC (through artificial lipid bilayers) and of trehalose (in actual RBC) are likely attributable to the same type of mechanism. This underlying mechanism is anticipated to be a consequence of formation of curvatures within the bilayer structure, which could lead to physical/biochemical changes in the membrane and allow increased transient permeability. The possibility of bilayer curvatures without membrane rupture has for example been reported, in other circumstances [47]. Moreover, hydroxyapatite nanoparticles (although of different composition) were shown to elicit formation of membrane curvatures in suspensions of RBC [31]. To deepen the examination of this point, we performed numerical simulations using the SCMF theory, where lipid molecules were modeled by a 3-beads model (one head bead H and two tail beads T) and apatite NP by a sphere, in a first approximation, in interaction with the heads of lipids (H). The launch of the computation evolved toward a local deformation of the bilayer (Fig. 7). This modeling thus suggests some degree of local destabilization/curving of the bilayer when apatite NP are present, which is in perfect agreement with our bilayer capacitance measurements showing a local alteration of the membrane physical/electrical properties when contacted with the NP (Fig. 6c and Figure S1 in Supporting Information). The formation of actual “nanopores” can however be excluded based on our experimental observations as no pores were detected by electrophysiological measurements (even at high NP concentration). Only a local modification of the 3D organization of the lipid molecules constituting the membrane is involved.

By momentarily and locally altering the lipid bilayer (in a reversible way since the bilayer remains experimentally stable over time), all these results concur to elucidate, both from experimental and computational viewpoints, the enhanced permeability noticed for low-molecular weight components like trehalose and FITC, when AEP/HMP colloidal apatite NP are present in the medium, thus explaining in turn the improved RBC cryosurvival data. As a final confirmation of these conclusions, the intracellular trehalose was titrated using a trehalose quantification kit after a developed cells lysis/trehalose extraction procedure. As expected (Fig. 4), the amount of trehalose quantified for RBC incubated in the presence of colloidal apatite NP was significantly increased as opposed to trehalose alone, which followed well the cryosurvival data (see Fig. 5).

4. Conclusion

Incubation of RBC with colloidal bio-inspired apatite NP in the co-presence of trehalose is reported here, for the first time, to dramatically increase the cryosurvival of RBC after freeze-thawing. RBC cryosurvival reached 91%, equivalent to the FDA-approved procedure using glycerol. A complementary set of data, based on experimental and computational results, concurred to show that AEP/HMP-stabilized apatite NP enhance the permeation of trehalose through the bilayer by locally interacting with the lipid bilayer. Trehalose translocation into RBC is facilitated via an indirect mechanism arising from NP/bilayer interactions (and not by the direct formation of temporary pores in the membrane). Results suggest that apatite NP enable the translocation of trehalose by locally modifying the 3D organization of the lipids in the interaction with NP, through transient breaching of the lipid bilayer.

To the best of our knowledge, this is the first report on the application of biocompatible inorganic compounds for cryopreservation applications. The massively increased survival of RBC after freeze-thawing coupled with the high biocompatibility of colloidal AEP/HMP-stabilized apatite NP and their low cost of production make such system a relevant alternative to commonly used toxic preservation agents (DMSO, glycerol), and show great promise for future applications in the cryopreservation of blood and mammal cells, and in biomedicine in general.

5. Experimental section

5.1. Preparation and characterization of bio-inspired apatite nanoparticles

Apatite colloidal suspensions were obtained as follows: bio-inspired non-stoichiometric nanocrystalline apatite $Ca_{10-x}(PO_4)_{6-x}(HPO_4,CO_3)_x(OH)_{2-x}$ was precipitated at room temperature from calcium nitrate and di-ammonium hydrogenphosphate in deionized water, at pH 9.5, and in the presence of 2-aminoethylphosphate $NH_3^+-CH_2-CH_2-O-P(O)(O^-)_2$ or "AEP" for agglomeration control; AEP being a biocompatible molecule encountered naturally in the composition of cell membranes (AEP represents the polar head of the phospholipid phosphatidylethanolamine) [48]. The AEP:Ca molar ratio in the reacting medium was set to 1:1. All reactants were of reagent grade. Solution A (6.25 mL) contained calcium nitrate tetrahydrate $Ca(NO_3)_2{\cdot}4H_2O$ (4.87 mmol), solution B (6.25 mL) contained AEP (4.87 mmol), and solution C (12.5 mL) contained di-ammonium hydrogenphosphate (1.62 mmol). Solution A was mixed with solution B under constant stirring, leading to solution D. The acidic pH of this resulting solution as well as that of solution C were adjusted to 9.5 by addition of few drops of concentrated ammonia. Mixing C and D allowed precipitation. The suspension was then allowed to mature in an oven preset at 100 °C for 16 h. When mentioned in the text, europium-doped apatite suspensions (containing luminescent Eu^{3+} ions as previously reported) [49] were also prepared by following the same protocol but replacing 1.5 mol.% of calcium nitrate in the starting medium by the same molar amount of europium (III) nitrate.

Each colloid (25 mL) was then purified by dialysis as previously described in detail [50]. Briefly, dialysis was carried out at room temperature using a tubular cellulose membrane (molecular weight cut-off: 6000–8000 Da) held vertically and introduced in 900 mL of dialysis medium (deionized water) under constant stirring. The dialysis medium was regularly exchanged with a fresh one after 4, 8, 22 and 26 h. Sodium hexametaphosphate $(NaPO_3)_6$ or "HMP" was added to the purified colloids for improving dispersibility and for lowering the suspension pH down to physiological value: addition of HMP was stopped when reaching pH ≅ 7.4. Afterwards, the colloids were freeze-dried for facilitating storage before use. Glucose, a hydrosoluble matrix, was added (15 mM) to the colloidal NP prior to freeze-drying for preventing uncontrolled aggregation and favoring the NP redispersion in the medium while preserving particle size distribution [32]. Before the start of experiments, each freeze-dried colloid was reconstituted with deionized water to reach the final NP concentration of 2.25 mg/mL and filtered through a 0.2 μm syringe-filter.

The apatite NP were characterized using different complementary techniques. Dynamic light scattering and zeta potential measurements were performed on a Zetasizer Nano ZS (Malvern Instruments, $\lambda = 630$ nm) and allowed to determine respectively the hydrodynamic diameter of the particles (so-called "particle size" in the remaining of the text) and their overall surface charge. The crystallographic structure of freeze-dried particles was investigated by X-ray diffraction (XRD) using a CPS 120 INEL diffractometer with the Kα Cobalt radiation (1.78892 Å). Fourier transform infrared (FTIR) spectroscopy analyses were run on a Nicolet 5700 spectrometer, in the wavenumber range 400–4000 cm^{-1} with a resolution of 4 cm^{-1}. Ca and Eu contents were checked by Induced Coupled Plasma Atomic Emission Spectroscopy, ICP-AES (relative uncertainty: 3%). The phosphate content was determined by spectrophotometry (Shimadzu UV 1800) at $\lambda = 460$ nm using the yellow phospho-vanado-molybdenum complex (relative uncertainty: 0.5%) [51]. The carbonation content was estimated from the relative integrated band intensities between the ν_3CO_3 and the $\nu_1\nu_3PO_4$ bands following the methodology previously published [52]. The AEP content associated to the colloidal nanoparticles was determined by nitrogen microanalysis (relative uncertainty 0.4%). Transmission electron microscopy (TEM) was run on a JOEL JEM-1011 set at 100 KeV. For these TEM observations, the suspensions were briefly sonicated (50 kHz, 30 s) and carbon-coated copper TEM-grid were rapidly dipped into the suspension and allowed to dry prior to analysis.

5.2. Incubation media

Four different incubation media were used in the study (Table 1). Incubation media with bio-inspired apatite NP (Apa6.5, Apa7.4) were prepared by dissolving NaCl, Hepes and trehalose (D-(+)-trehalose dihydrate) powder in the fresh aqueous suspension of reconstituted apatite NP suspension ($c = 2.25$ mg/mL). Afterwards, the pH of the medium was adjusted with NaOH/HCl using a digital pH meter (FE20, Mettler Toledo, Switzerland). All chemicals were purchased from Sigma Aldrich, UK. In the study, the concentration of trehalose was determined to have relatively high concentration of trehalose but still in the range that would not provoke hemolysis due to osmolarity excess. In this context, 0.35 M trehalose and total osmolarity of 600 mOsm were selected as relevant conditions in these incubation experiments. The apatite NP concentration was fixed to 2.25 mg/mg so as to remain lower than the 3 mg/mL limit noticed during bilayer formation in our model system (free-standing lipid bilayers). The pH values used in this work (6.5 and 7.4) were selected so as to have enough difference between the two values to get evidence of possible modifications while avoiding too acidic conditions being detrimental to non-stoichiometric apatites (partial dissolution) and to RBC (potential hemolysis).

5.3. Preparation of RBC

RBC were isolated from the fresh whole sheep blood supplied in Alsever's medium (TCS Biosciences Ltd, UK) and used within two days. Before use, RBC were washed with physiological 0.9% NaCl solution (Table 1), centrifuged (at 600 g for 15 min) and then the

supernatant was discarded. Two more NaCl washes were performed before use.

5.4. Loading of RBC with trehalose

Washed RBC were divided into 0.5 mL samples of approximately 10% packed cell volume (hematocrit) and centrifuged at 600 g for 2 min. Their supernatants were discarded and 0.45 mL of incubation medium (Table 1) was added to yield a final RBC concentration of approximately 10% hematocrit, or approximately $3{\cdot}10^8$ RBC mL^{-1}. Resulting mixtures were homogenously re-suspended and incubated in an air bath incubator (Binder UK; Wolverhampton, UK) for 7 h at 37 °C and slowly rotated (Maplelab Scientific Ltd, UK) at 10 rpm. The incubation duration of 7 h was selected here on the basis of previous studies by Lynch and Slater et al. on the cryopreservation of RBC and intracellular delivery of trehalose [53–55]. Cell count was performed both at the start and at the end of incubation using a hemocytometer (Hawksley, UK).

5.5. Quantification of intracellular trehalose

An experimental procedure was set up here to allow the quantification of intracellular trehalose. This procedure involved several successive steps: 1) Incubation of RBC in incubation media (Table 1) for 7 h (for trehalose alone, both pH values 6.5 and 7.4 were here tested); 2) After gentle centrifugation (i.e. 250 rpm) the trehalose-rich supernatant was discarded and the remaining cell pellet was washed with large volume of cold NaCl iso-osmotic to the incubation medium (~600 mOsm) to remove extracellular trehalose. The suspension was centrifuged again and the NaCl supernatant was discarded. The obtained cell suspension was used for quantification of trehalose. 3) 300 mm^3 of deionized water were added to the RBC pellet to lyse the cells and then mixed with 5 mL 80% methanol for trehalose extraction. The mixture was incubated in the ultrasound bath at 80 °C for 2 h under constant sonication. Samples were then centrifuged at 3000 g for 10 min and the methanol supernatants were collected separately in tubes. These supernatants were then evaporated in an oven set at 80 °C overnight to leave dry trehalose residues in tubes. This procedure, from methanol addition to evaporation, was then repeated one more time. After final evaporation, the tubes with trehalose residues were kept in a freezer until further analysis. 4) For the quantification of trehalose, 600 mm^3 of milli-Q water were added to the tubes with dry trehalose residues. The tubes were then vortexed/sonicated several times at elevated temperature (~50 °C) for ~ 30 min to ensure that all trehalose was dissolved. Trehalose content was then quantified using the trehalose assay kit (Megazyme, USA) according to manufacturer instructions and by using the microplate assay procedure (Synergy H1, USA). To ensure that reported values are only due to intracellular trehalose, negative controls were put in place. Incubating RBC in corresponding incubation media for ~1 min and then passing them through the trehalose measurement protocol allowed determination of the amount of measured trehalose due to extracellular trehalose incompletely removed during washing. The negative controls were used for each incubation media and all reported loading values are relative to their corresponding negative control values. Intracellular concentration of trehalose was calculated according to the following equation:

$$C = \frac{n(trehalose)}{V(\text{intracellular})} = \frac{n(trehalose)}{MCV \cdot N \cdot v} \quad (3)$$

where C [mM] is the concentration of intracellular trehalose, n(trehalose) [moles] is the measured amount of trehalose and V(intracellular) is the total intracellular volume in a sample that is occupied by water and available to trehalose and other solutes. n(trehalose) was determined by multiplying the measured concentration of trehalose by the volume of water added in the tube (600 mm^3). V(intracellular) was calculated for each sample by multiplying the number of RBC contained in the suspension (concentration ~ 2.5×10^9 cells mL^{-1}) by the mean cell volume (MCV) of RBC in the incubation medium (~30×10^{-15} L). The value was multiplied by 0.7 to account for the fact that only 70% of the intracellular RBC volume is accessible to water, as the remaining 30% is occupied by membranes [56]. MCV of RBC incubated in different media has been measured via microhematocrit. After incubation period, RBC suspensions with known cell concentration were centrifuged in 70 mm microhematocrit tubes at 6000 g (Domel Centric 150, Slovenia) for 10 min according to the manufacturer's instructions and then packed cell volume (hematocrit) was determined. MCV was then calculated by dividing the hematocrit with the cell concentration. The calculated MCV of RBC in different media were as follows: 3.2×10^{-14} L (medium “0,9% NaCl”); 3.0×10^{-14} L (media “Apa6.5” and “Trehalose pH 6.5”); 2.5×10^{-14} L (media “Apa7.4” and “Trehalose pH 7,4”).

5.6. Hemolysis assay

Hemolysis of RBC after incubation in the different media (Table 2) was evaluated by measuring hemoglobin absorbance at 541 nm using a spectrophotometer (SP75, Sanyo, Japan). The Drabkin's method for hemoglobin assay was not employed because methemoglobin concentration was insignificant after incubation at all steps of trehalose loading (data not shown) [13]. Washed RBC were used to create a calibration curve relating RBC mL^{-1}, counted using a hemocytometer (Hawksley, UK), to hemoglobin absorbance after the lysis of those cells. Initial cell count (cell count of samples before incubation or freezing and thawing) was evaluated by lysing control samples with deionized water via hypotonic osmotic shock and measuring hemoglobin absorbance. The number of cells that lysed during experimentation was evaluated by centrifuging samples after experimentation and measuring the hemoglobin absorbance of the supernatant. Percent hemolysis was then calculated as follows:

$$hemolysis(\%) = 100 \cdot \frac{lysed\ cell\ count\ after\ incubation}{initial\ cell\ count} \quad (4)$$

5.7. RBC cryosurvival evaluation

RBC were incubated at approximately 10% hematocrit in either 0.9% NaCl, 0.35 M trehalose or 0.35 M trehalose + apatite NP (pH 6.5 and 7.4), each for 7 h at 37 °C. The complete compositions of the different media used in this study are listed in Table 1. In addition to Hepes, glucose is present due to the redispersion of freeze-dried apatite NP. The cryopreservation protocol utilized relatively rapid freezing and thawing: freezing was accomplished by direct immersion of samples in liquid nitrogen as described [13], a method similar to the one with a freezing rate that has been estimated at 265 ± 12 °C min^{-1} [15]. After immersion in liquid nitrogen samples were transferred to a freezer at −80 °C for a minimum one day. Thawing was accomplished by warming samples in a 37 °C water bath. After thawing, cell number in suspensions was determined using a hemocytometer. Percent survival of RBC after cryopreservation was calculated based on normalization to pre-freeze cell number:

$$cryosurvival\,(\%) = 100 \cdot \frac{cell\ count\ after\ freezing\ and\ thawing}{cell\ count\ after\ incubation} \quad (5)$$

5.8. Study of interaction between apatite NP and model membranes in a microfluidic device

A microfluidic device was used to study the mechanism of interaction between apatite NP (possibly doped with europium) and model lipid membranes, and to follow the possible translocation of Eu-doped apatite and of a fluorescent trehalose substitute (FITC) through the membrane barrier. FITC is a hydrophilic membrane-impermeable organic dye with similar molecular weight as trehalose, and was used as a fluorescent tracer and trehalose substitute to study molecular translocation through the membrane barrier. The device consists of a cross geometry made of micro-channels with rectangular cross section fabricated by soft lithography (5a). Channel dimensions were 200−300 μm in width and 140 μm in height. The device was molded against a SU-8 photo resist master on a silicon wafer using poly(dimethylsiloxane) (PDMS) (Sylgard 184, Dow Corning, USA). The surface of the PDMS devices was exposed to plasma (Diener electronic GmbH, Germany) and sealed with a plasma-treated glass cover slide. The sealed device was rendered hydrophilic by heating to 135 °C overnight. The liquids were dispensed from syringes (Hamilton Bonaduz AG, Switzerland) connected to the microfluidic device via Teflon tubing. A homemade computer-operated syringe pump was used to control the injection of the water and oil phases.

Several types of lipids were used to form lipid bilayers, namely phosphatidylcholines DOPC (1,2-Dioleoyl-sn-glycero-3-phosphocholine) and DPHPC (1,2-diphytanoyl-sn-glycero-3-phosphocholine) and monoolein (2,3-Dihydroxypropyl oleate). When mentioned in the text (section on FITC diffusion), a more complex lipid composition was additionally used for mimicking the membrane composition of RBC, and inspired from a reported composition [57]; it was composed of DOPC 29% - sphingomyelin (SM) 25% - lysophosphatidylcholine (LPC) 1% - phosphatidylserine (DOPS) 15% - phosphatidylinositol (PI) 0.5% - phosphatidic acid (PA) 1% - phosphatidylethanolamine (DOPE) 28.5%. This lipid composition will be referred to as “Red Blood Cell-like” in the text.

All lipids used in this study were purchased at Avanti Polar Lipid (USA).

5.9. Formation of an unsupported lipid bilayer

A variant of the Droplet Interface Bilayer (DiB) technique was used to produce a free standing lipid membrane in a microfluidic chip [37,38]. Using a volume-controlled system with syringe pumps, two fingers of an aqueous phase containing 100 mM NaCl were injected face-to-face into microchannels with a cross-geometry which were previously filled with squalene as oily solution containing the lipid continuous phase (monoolein or DOPC) (Fig. 6a). After few seconds, the water-oil interface of each finger was covered with a monolayer of lipid molecules. Once two liquid fingers were brought in contact, the two lipid monolayers interact and form a lipid bilayer within a short time. This process is not instant; it occurs by the drainage of the oil present between the two lipid monolayers, during the so-called zipping process. After its formation, the bilayer is stable and can be analyzed simultaneously by optical microscopy and electrophysiological experiments.

5.10. Two-droplets system to monitor Eu-doped apatite NP or FITC diffusion via epifluorescence microscopy

Investigation of Eu-doped apatite NP or of FITC diffusion through model membranes was performed using a novel “two-droplets” system. The system is composed of two droplets separated by a lipid bilayer (monoolein or DOPC or asymmetric DOPC/DPHPC). One droplet is typically composed of a medium (either Apa6.5 or Apa6.5) containing the NP (0.1 ng/mL to 1 mg/mL) and FITC (2 mM) when mentioned in the text, while the second droplet is composed of the same medium but without NP nor FITC. By observing both droplets by epifluorescence microscopy we could investigate the possible transfer of Eu-doped apatite NP or FITC through the lipid bilayer.

5.11. Electrophysiological measurements of the lipid membrane

The electrophysiological properties of the bilayer were analyzed using a patch-clamp amplifier (EPC 10 USB - HEKA). Ag/AgCl electrodes were prepared by inserting a silver chloride wire in a borosilicate glass pipette (outer diameter 1.5 mm, inner diameter 0.86 mm, VWR) containing an electrolyte agarose solution. Lipid membrane capacitance was measured using the Lock-In function provided by the patch-clamp amplifier.

5.12. Imaging of fluorescent apatite NP and FITC

Epifluorescence microscopy was used to detect the fluorescence signal emitted from the Eu-doped apatite NP or from FITC. To this aim, a commercial particle image velocimetry setup from LaVision (Germany) was used which is based on an inverted epifluorescence microscope (Zeiss Axio Observer-Z1). Eu-doped NP were observed under UV illumination at 256 nm (Newport, USA), and FITC molecules were followed under blue laser (473 nm) illumination.

5.13. Computational modeling of the NP/bilayer interaction

The interaction between the surface of a typical lipid bilayer and one apatite nanoparticle was investigated using the Single Chain Mean Field (SCMF) theory, described previously in the literature [42,43]. In a 3-beads model, the lipid bilayer is then represented by the fields of lipid tails (T) and heads (H), which can rearrange due to local environment and interactions with external objects. In a simplified approach, the apatite NP considered spherical was modeled as adsorbing to lipid heads (H) through the negative interaction parameter ε_H, this parameter characterizing the attraction of lipid heads H to the NP. In these simulations, the fully-parametrized DMPC lipid composition was selected. Results can however be extended to other lipid compositions (like DOPC for instance) since the 3-beads model is a coarse-grained model and does not allow distinguishing behavioral differences at the nanoscale.

Acknowledgements

M.S. and V.B. acknowledge funding from Marie Curie Actions under EU FP7 Initial Training Network SNAL 608184. H.T, R.S and J.B. F. acknowledge funding from SFB1027 (DFG). The authors would also like to thank Dr Krish Mahbubani (University of Cambridge) for valuable discussions.

Appendix A. Supplementary data

Supplementary data related to this article can be found at http://dx.doi.org/10.1016/j.biomaterials.2017.06.018.

References

[1] J.W. Lagerberg, Cryopreservation of red blood cells, Methods Mol. Biol. 1257 (2015) 353–367.
[2] K.L. Scott, J. Lecak, J.P. Acker, Biopreservation of red blood cells: past, present, and future, Transfus. Med. Rev. 19 (2) (2005) 127–142.
[3] C.R. Valeri, G. Ragno, Cryopreservation of human blood products, Transfus. Apher. Sci. 34 (3) (2006) 271–287.
[4] C.J. Capicciotti, J.D.R. Kurach, T.R. Turner, R.S. Mancini, J.P. Acker, R.N. Ben, Small molecule ice recrystallization inhibitors enable freezing of human red blood cells with reduced glycerol concentrations, Sci. Rep. 5 (2015) 9692.
[5] C.N. Chaudhari, Frozen red blood cells in transfusion, Med. J. Armed Forces India 65 (1) (2009) 55–58.
[6] V. Pallotta, G.M. D'Amici, A. D'Alessandro, R. Rossetti, L. Zolla, Red blood cell processing for cryopreservation: from fresh blood to deglycerolization, Blood Cells, Mol. Dis. 48 (4) (2012) 226–232.
[7] P. Mazur, Stopping biological time. The freezing of living cells, Ann. N. Y. Acad. Sci. 541 (1988) 514–531.
[8] J.E. Lovelock, The mechanism of the protective action of glycerol against haemolysis by freezing and thawing, Biochim. Biophys. Acta 11 (1) (1953) 28–36.
[9] I.B. Bakaltcheva, C.O. Odeyale, B.J. Spargo, Effects of alkanols, alkanediols and glycerol on red blood cell shape and hemolysis, Biochim. Biophys. Acta (BBA) - Biomembr. 1280 (1) (1996) 73–80.
[10] W. Asghar, R. El Assal, H. Shafiee, R.M. Anchan, U. Demirci, Preserving human cells for regenerative, reproductive, and transfusion medicine, Biotechnol. J. 9 (7) (2014) 895–903.
[11] A. Tinmouth, D. Fergusson, I.C. Yee, P.C. Hebert, Clinical consequences of red cell storage in the critically ill, Transfusion 46 (11) (2006) 2014–2027.
[12] R.C. Deller, M. Vatish, D.A. Mitchell, M.I. Gibson, Synthetic polymers enable non-vitreous cellular cryopreservation by reducing ice crystal growth during thawing, Nat. Commun. 5 (2014) 3244.
[13] A.L. Lynch, R. Chen, P.J. Dominowski, E.Y. Shalaev, R.J. Yancey Jr., N.K.H. Slater, Biopolymer mediated trehalose uptake for enhanced erythrocyte cryosurvival, Biomaterials 31 (23) (2010) 6096–6103.
[14] C. Pellerin-Mendes, L. Million, M. Marchand-Arvier, P. Labrude, C. Vigneron, In Vitro Study of the protective effect of trehalose and dextran during freezing of human red blood cells in liquid nitrogen, Cryobiology 35 (2) (1997) 173–186.
[15] J.L. Holovati, M.I.C. Gyongyossy-Issa, J.P. Acker, Effects of trehalose-loaded liposomes on red blood cell response to freezing and post-thaw membrane quality, Cryobiology 58 (1) (2009) 75–83.
[16] A.D. Elbein, Y.T. Pan, I. Pastuszak, D. Carroll, New insights on trehalose: a multifunctional molecule, Glycobiology 13 (2003) 17–27.
[17] J.H. Crowe, L.M. Crowe, Preservation of mammalian cells-learning nature's tricks, Nat. Biotech. 18 (2) (2000) 145–146.
[18] R. Shirakashi, C.M. Köstner, K.J. Müller, M. Kürschner, U. Zimmermann, V.L. Sukhorukov, Intracellular delivery of trehalose into mammalian cells by electropermeabilization, J. Membr. Biol. 189 (1) (2002) 45–54.
[19] S.M. Moghimi, A.C. Hunter, J.C. Murray, Nanomedicine: current status and future prospects, Faseb J. 19 (3) (2005) 311–330.
[20] P. Prabhu, V. Patravale, The upcoming field of theranostic nanomedicine: an overview, J. Biomed. Nanotechnol. 8 (6) (2012) 859–882.
[21] V. Sokolova, M. Epple, Inorganic nanoparticles as carriers of nucleic acids into cells, Angew. Chem. Int. Ed. 47 (8) (2008) 1382–1395.
[22] A. Al-Kattan, V. Santran, P. Dufour, J. Dexpert-Ghys, C. Drouet, Novel contributions on luminescent apatite-based colloids intended for medical imaging, J. Biomater. Appl. 28 (5) (2014) 697–707.
[23] C. Drouet, A. Al-Kattan, M. Choimet, A. Tourrette, V. Santran, J. Dexpert-Ghys, B. Pipy, F. Brouillet, M. Tourbin, Biomimetic apatite-based functional nanoparticles as promising newcomers in nanomedicine: overview of 10 years of initiatory research, HSOA J. General Pract. Med. Diagn. (GPMD) 1 (1) (2015) 1–9.
[24] M. Iafisco, E. Varoni, M. Di Foggia, S. Pietronave, M. Fini, N. Roveri, L. Rimondini, M. Prat, Conjugation of hydroxyapatite nanocrystals with human immunoglobulin G for nanomedical applications, Colloids Surfaces B-Biointerfaces 90 (2012) 1–7.
[25] J. Gomez-Morales, M. Iafisco, J. Manuel Delgado-Lopez, S. Sarda, C. Drouet, Progress on the preparation of nanocrystalline apatites and surface characterization: overview of fundamental and applied aspects, Prog. Cryst. Growth Charact. Mater. 59 (1) (2013) 1–46.
[26] M. Iafisco, J. Manuel Delgado-Lopez, E.M. Varoni, A. Tampieri, L. Rimondini, J. Gomez-Morales, M. Prat, Cell surface receptor targeted biomimetic apatite nanocrystals for cancer therapy, Small 9 (22) (2013) 3834–3844.
[27] V.V. Sokolova, I. Radtke, R. Heumann, M. Epple, Effective transfection of cells with multi-shell calcium phosphate-DNA nanoparticles, Biomaterials 27 (16) (2006) 3147–3153.
[28] A. Bouladjine, A. Al-Kattan, P. Dufour, C. Drouet, New advances in nanocrystalline apatite colloids intended for cellular drug delivery, Langmuir 25 (20) (2009) 12256–12265.
[29] A. Al-Kattan, S. Girod-Fullana, C. Charvillat, H. Ternet-Fontebasso, P. Dufour, J. Dexpert-Ghys, V. Santran, J. Bordere, B. Pipy, J. Bernad, C. Drouet, Biomimetic nanocrystalline apatites: emerging perspectives in cancer diagnosis and treatment, Int. J. Pharm. 423 (1) (2012) 26–36.
[30] M. Bonazzi, P. Cossart, Bacterial entry into cells: a role for the endocytic machinery, FEBS Lett. 580 (12) (2006) 2962–2967.
[31] Y. Han, X. Wang, H. Dai, S. Li, Nanosize, Surface Charge, Effects of hydroxyapatite nanoparticles on red blood cell suspensions, ACS Appl. Mater. Interfaces 4 (9) (2012) 4616–4622.
[32] M. Tourbin, A. Al-Kattan, C. Drouet, Study on the stability of suspensions based on biomimetic apatites aimed at biomedical applications, Powder Technol. 255 (2014) 17–22.
[33] M. Choimet, K. Hyoung-Mi, O. Jae-Min, A. Tourrette, C. Drouet, Nanomedicine: interaction of biomimetic apatite colloidal nanoparticles with human blood components, Colloids Surfaces B Biointerfaces 145 (2016) 87–94.
[34] C. Drouet, Apatite formation: why it may not work as planned, and how to conclusively identify apatite compounds, Biomed Res. Int. (2013) 12.
[35] C. Rey, O. Marsan, C. Combes, C. Drouet, D. Grossin, S. Sarda, Characterization of calcium phosphates using vibrational spectroscopies, in: B. Ben-Nissan (Ed.), Advances in Calcium Phosphate Biomaterials, Springer, Berlin Heidelberg, 2014, pp. 229–266.
[36] R. Legros, N. Balmain, G. Bonel, Age-related changes in mineral of rat and bovine cortical bone, Calcif. Tissue Int. 41 (3) (1987) 137–144.
[37] H. Bayley, B. Cronin, A. Heron, M.A. Holden, W.L. Hwang, R. Syeda, J. Thompson, M. Wallace, Droplet interface bilayers, Mol. Biosyst. 4 (12) (2008) 1191–1208.
[38] J.N. Vargas, R. Seemann, J.-B. Fleury, Fast membrane hemifusion via dewetting between lipid bilayers, Soft Matter 10 (46) (2014) 9293–9299.
[39] R.P. Carney, Y. Astier, T.M. Carney, K. Voïtchovsky, P.H. Jacob Silva, F. Stellacci, Electrical method to quantify nanoparticle interaction with lipid bilayers, ACS Nano 7 (2) (2013) 932–942.
[40] M.A. Al-Anber, Thermodynamics - interaction studies - solids, liquids and gases, in: J.C. Moreno-Pirajan (Ed.), InTech, 2011, pp. 737–764.
[41] K. Hammami, H.E. Feki, O. Marsan, C. Drouet, Adsorption of nucleotides on biomimetic apatite: the case of adenosine 5′ monophosphate (AMP), Appl. Surf. Sci. 353 (0) (2015) 165–172.
[42] S. Pogodin, V.A. Baulin, Coarse-grained models of phospholipid membranes within the single chain mean field theory, Soft Matter 6 (10) (2010) 2216–2226.
[43] Y. Guo, S. Pogodin, V.A. Baulin, General model of phospholipid bilayers in fluid phase within the single chain mean field theory, J. Chem. Phys. 140 (17) (2014) 174903.
[44] D. Gao, J.K. Critser, Mechanisms of cryoinjury in living cells, ILAR J. 41 (4) (2000) 187–196.
[45] A. Grunenwald, C. Keyser, A.M. Sautereau, E. Crubezy, B. Ludes, C. Drouet, Adsorption of DNA on biomimetic apatites: toward the understanding of the role of bone and tooth mineral on the preservation of ancient DNA, Appl. Surf. Sci. 292 (2014) 867–875.
[46] C.E. Stanley, K.S. Elvira, X.Z. Niu, A.D. Gee, O. Ces, J.B. CEdel, A.J. deMello, A microfluidic approach for high-throughput droplet interface bilayer (DIB) formation, Chem. Commun. 46 (10) (2010) 1620–1622.
[47] L. Iversen, S. Mathiasen, J.B. Larsen, D. Stamou, Membrane curvature bends the laws of physics and chemistry, Nat. Chem. Biol. 11 (11) (2015) 822–825.
[48] L. Rothfield, A. Finkelstein, Membrane biochemistry, Annu. Rev. Biochem. 37 (1968) 463–496.
[49] A. Al-Kattan, P. Dufour, J. Dexpert-Ghys, C. Drouet, Preparation and physicochemical characteristics of luminescent apatite-based colloids, J. Phys. Chem. C 114 (7) (2010) 2918–2924.
[50] A. Al-Kattan, P. Dufour, C. Drouet, Purification of biomimetic apatite-based hybrid colloids intended for biomedical applications: a dialysis study, Colloids Surfaces B-Biointerfaces 82 (2) (2011) 378–384.
[51] A. Gee, V.R. Dietz, Determination of phosphate by differential spectrophotometry, Ann. Chem. 25 (1953) 1320–1324.
[52] A. Grunenwald, C. Keyser, A.M. Sautereau, E. Crubézy, B. Ludes, C. Drouet, Revisiting carbonate quantification in apatite (bio)minerals: a validated FTIR methodology, J. Archaeol. Sci. 49 (2014) 134–141.
[53] A.L. Lynch, N.K.H. Slater, Influence of intracellular trehalose concentration and pre-freeze cell volume on the cryosurvival of rapidly frozen human erythrocytes, Cryobiology 63 (1) (2011) 26–31.
[54] A.L. Lynch, R. Chen, P.J. Dominowski, E.Y. Shalaev, R.J. Yancey Jr., N.K.H. Slater, Biopolymer mediated trehalose uptake for enhanced erythrocyte cryosurvival, Biomaterials 31 (23) (2010) 6096–6103.
[55] A.L. Lynch, R. Chen, N.K. Slater, pH-responsive polymers for trehalose loading and desiccation protection of human red blood cells, Biomaterials 32 (19) (2011) 4443–4449.
[56] E. Gianolio, G. Ferrauto, E. Di Gregorio, S. Aime, Re-evaluation of the water exchange lifetime value across red blood cell membrane, Biochim. Biophys. Acta (BBA) - Biomembr. 1858 (4) (2016) 627–631.
[57] J.A. Virtanen, K.H. Cheng, P. Somerharju, Phospholipid composition of the mammalian red cell membrane can be rationalized by a superlattice model, Proc. Natl. Acad. Sci. 95 (9) (1998) 4964–4969.